Micronecking Operative during Crazing in Polymer Glasses

Arnold C.-M. Yang,* Martin S. Kunz, and J. A. Logan

IBM Research Division, Almaden Research Center, 650 Harry Road, San Jose, California 95120-6099

Received October 6, 1992; Revised Manuscript Received November 11, 1992

ABSTRACT: The topography of crazes in polystyrene films was studied by scanning force microscopy (SFM), and evidence of micronecking operative during crazing was observed. It was found that crazing not only generates fibrillar structures but also creates an unexpectedly large surface depression in the crazed regions. The depression was found to initially increase linearly with the craze width but leveled off to approximately 35% of the original film thickness when the craze width became larger than a critical width w_c. This behavior is independent of strain rate, aging time and the total applied deformation. The micronecking process during crazing indicates that the newly drawn fibrils were continuously deformed even after the fibrillation. Due to the large depression, the surface-to-surface distance between the craze fibrils is much smaller than that previously realized. This discovery may help to explain the fast fibril coalescence at room temperature and to examine the process of solvent-induced crazing. The mechanics of craze initiation and breakdown were then studied on the basis of necking theories of Considere construction and Bridgman's plasticity theory. The results from the stress analysis are in excellent agreement with the fibril breakdown behavior observed experimentally.

Introduction

The phenomenon of crazing, i.e., the formation of narrow fibrillated regions surrounded by elastically deformed material in stretched polymer glasses, is of paramount importance because it is responsible for the brittle failures in glassy polymers.[1-16] Crazes have been extensively studied in the past, particularly by transmission electron microscopy (TEM), and it was commonly accepted that the formation of the craze fibrils is probably by a surface drawing mechanism. Namely, a craze widens by drawing fresh material from the "active zones",[9] the narrow regions of softened material at the craze/bulk boundaries, and once the fibrils are drawn into the craze, the fibrils thereafter maintain their geometry, spacing, and the state of deformation. However, the information obtained by TEM is flawed by the fact that the data are a two-dimensional projection of a three-dimensional structure in which the information about the spatial distribution of features in the viewing direction is missing. We have recently used scanning force microscopy (SFM), which allows very high resolution in all three dimensions, to study the craze topography. This paper reports the three-dimensional structure of crazes in polystyrene films for the first time and showed evidence of a different mechanism that also is operative during crazing. As strongly suggested by the SFM data, craze growth follows a micronecking process. This result not only sheds light into the fundamental crazing mechanisms but also provides new information regarding the mechanics of craze initiation, growth, and breakdown.

Experimental Techniques

A monodisperse polystyrene (PS; $M_w/M_n = 1.06$) of molecular weight $M_w = 2\,000\,000$ from Pressure Chemicals Co. was used in all experiments reported here. The polymer films were spin cast from toluene solutions onto clean glass slides. Films of three different thicknesses were prepared: 0.12, 0.55, and 2.6 μm. The thickness was measured by a profilometer (Alpha-step, Tencor Instruments) and was cross checked by using techniques of ellipsometry (Auto EL) and SFM (Nanoscope, Digital Instruments). The polystyrene film was floated off the substrate on distilled water and bonded onto supporting copper grids.[6] The PS films were deformed by stretching the copper grids to grow crazes in the films using a hand-operated strain jig or, for a better control of strain rate, a Minimat II Mechanical Tester (Polymer Lab Inc.). Immediately after crazing (usually within 1 h), the films were imaged and studied by the SFM as well as by a transmission electron microscope (TEM).

For scanning force microscopy, a contact mode SFM (Nanoscope II, Digital Instruments, Inc.) was used. All SFM imaging was done at ambient conditions. The SFM tip diameter of the Si_3N_4 cantilever (Microprobes, from Digital Instruments), estimated from the SEM images, was around 30–40 nm. During the SFM scanning, the axis of the cantilever was tilted with a fixed angle of approximately 10° with respect to the plane of scanning. Due to the tip geometry, the measurement of the topographic slopes was limited by the tip face angles α and β, as shown in Figure 1. The maximum measurable slope of the topographic features was 65°. However, except for the very narrow crazes, the depth measurements in the crazes were not limited by this tip geometry. In order to minimize any tip-induced damages, the smallest contact force was used. Usually a minimum contact force of approximately 140 nN was required to scan across the craze boundaries. The scan rate was between 1 and 2 Hz. Calibration for the in-plane length measurements was carried out with a diffraction grating whereas the height was calibrated using a series of VLSI standards. The TEM used was a Philips 400T (Philips, Eindhoven, The Netherlands). The microscope was operated at 100 kV and calibrated with a cross grating.

Results

1. General Craze Topography. When a PS film was stretched uniaxially at room temperature, crazes developed.[1-6] Figure 2 shows a typical topography obtained by SFM on crazes in a stretched PS film. A huge depression was observed at the craze region. The depression was found to increase linearly with the craze width and eventually reached a plateau of approximately 35% of the original film thickness. The depth measurement by SFM was confirmed by an independent measurement using a TEM shadowing technique.[17,18] In that experiment, a crazed PS film was coated with tiny Pt–Pd particles (ca. 2 nm) by evaporating the alloy at a fixed angle of 10° between the particle beam and the film surface. Due to the depression, a "shadow" formed inside the crazes, as shown in Figure 3. It is clear that the craze length had to be oriented perpendicular to the particle beam in order to measure the correct values for the shadow length. By

* To whom correspondence should be addressed. Present address: National Tsing Hua University, Department of Materials Science, Hsinchu, Taiwan, R.O.C.

0024-9297/93/2226-1767$04.00/0 © 1993 American Chemical Society

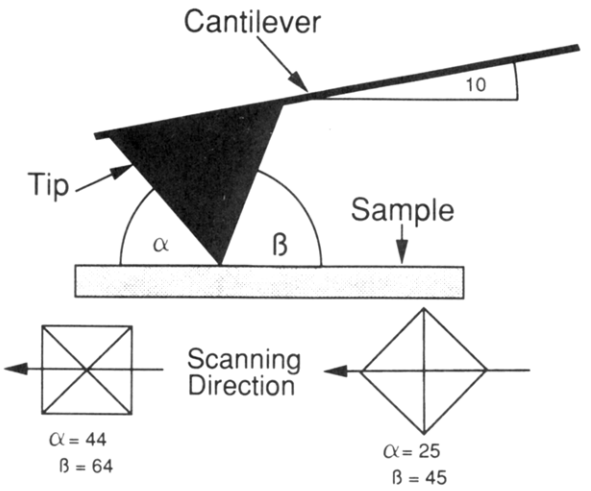

Figure 1. Geometry of the tip used in Nanoscope II.

measuring the shadow length from the TEM images, the depression depths were calculated using the equation $d = S \tan \alpha$ (Figure 3). As shown in Figure 4, excellent agreement was obtained between SFM and TEM results. This agreement indicates that the SFM measurements are not effected by the contact force used in the scanning.

The fine craze fibril features, however, were quite sensitive to the scan contact force under certain conditions. Although the fibril topography was insensitive to the scans in the parallel direction (to the craze fibrils), permanent tip-induced damages were noticed when scans in the normal direction proceeded. Figure 5a shows a craze image obtained by scanning in the parallel direction. This image was quite reproducible even after 30 scans at the same spot. The average period of surface fluctuation perpendicular to the fibril direction was determined from this image (Figure 5a) to be around 50 nm, on the same order of magnitude as that of fibril spacing reported by X-ray and TEM.[8,12-14] However, the period of surface fluctuation increased from 50 to 80 nm as the scans in the normal direction continued. Figure 5b shows a craze image after 25 times in the normal direction, where the tip-induced fibril aggregation is evident.

Due to a convolution effect from the finite SFM tip diameter, unfortunately the fibril diameters cannot be evaluated as clearly as fibril spacing. However, in the present case we can estimate the fibril diameters from the height difference on the surface by assuming that some of the fibrils are imaged as if they are lying on top of a flat surface. In that case, the height of the fibril corresponds to its diameter. The observed heights are in the range of 6–10 nm (Figure 5a) and are in very good agreement with values reported in the literature.[8,12-14]

2. Micronecking during Craze Growth. Figure 6 shows the craze depression plotted against the craze width for films of different thickness. A universal behavior was found for all the film thicknesses investigated. The depression was found to increase linearly as the craze widened. It leveled off, however, when the craze width w became larger than a critical width w_c. The level-off value of the depression is unexpectedly high, approximately 30–40% of the original film thickness. If the craze depression is assumed to be identical on the other side of the film, the total thickness in the crazed regions with $w \geq w_c$ is only ca. 30% of that of the film. Taking the volume fraction in the crazes to be around 0.2–0.25, as determined by TEM microdensitometry,[4,6,7] the fibril packing density in the crazes can be as high as the closest packing density of parallel cylinders (ca. 70%).

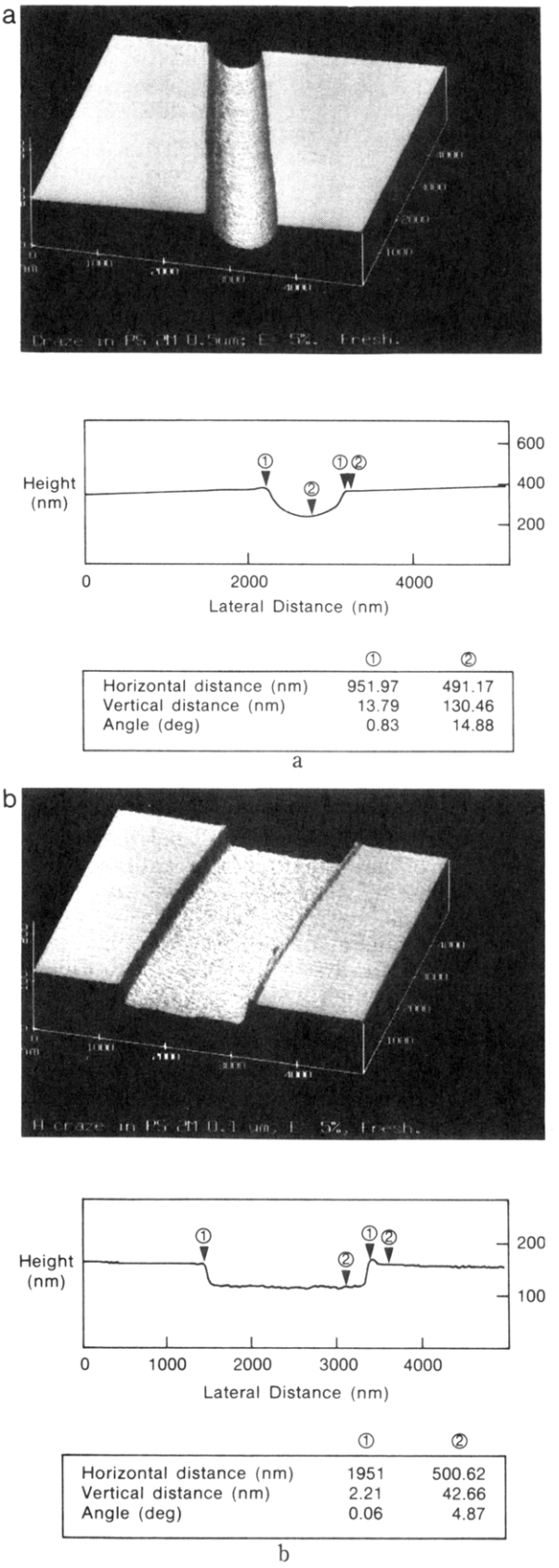

Figure 2. SFM topography across a typical craze: (a) a narrow craze ($w < w_c$); (b) a wide craze ($w > w_c$).

The maximum craze depression, when normalized to the original film thickness, is independent of the film thickness. The critical width w_c, however, increases almost linearly with the film thickness. As shown in Figure 6, w_c is approximately 4–5 times the film thickness. However, as the film thickness increased, it was impossible to obtain

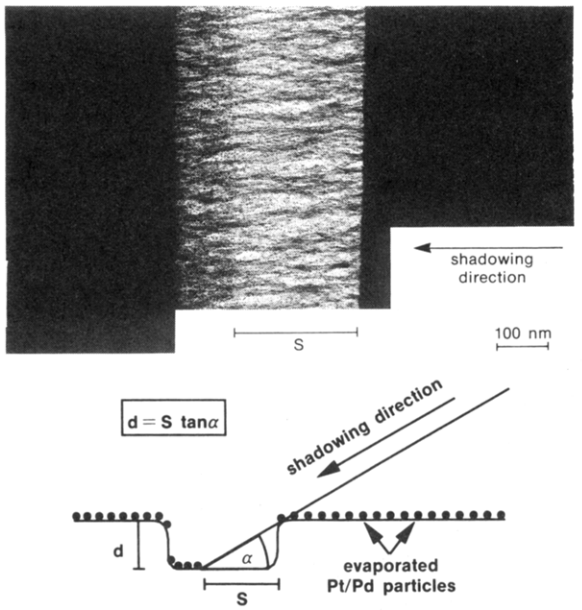

Figure 3. TEM micrograph of a craze shadowed with tiny Pt–Pd particles.

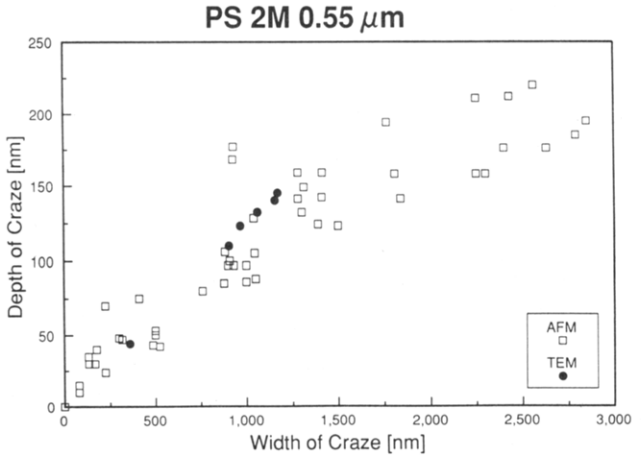

Figure 4. Depressions measured by the TEM shadowing technique compared with the data by SFM scanning.

wide crazes which were mechanically stable. In the bulk specimens, crazes usually broke down before reaching w_c. As will be shown later, this observation can be explained by a stress increase within the craze with the sample thickness.

It is difficult to measure the width of the shoulder at the craze/bulk boundaries. However, the shoulder width was found to be approximately constant with the craze width but increases linearly with the film thickness.

From Figure 7, where craze depression is shown versus the craze width for different applied strains, it is clear that the total applied strain essentially has no effect on the craze depression. It indicates that craze depth is not controlled by the total amount of deformation in the specimen; rather it is controlled by the actual width of the craze. Similarly, no effects were observed due to the strain rate and room temperature aging, as demonstrated in Figure 8.

The universal behavior of craze depression with craze width indicates a necking process during craze growth. Contradictory to that predicted by the surface drawing mechanism, clearly, as a craze widens, the newly drawn fibrils are still being deformed continuously even after fibrillation. This continuous deformation results in a contraction in the craze regions, creating a depression.

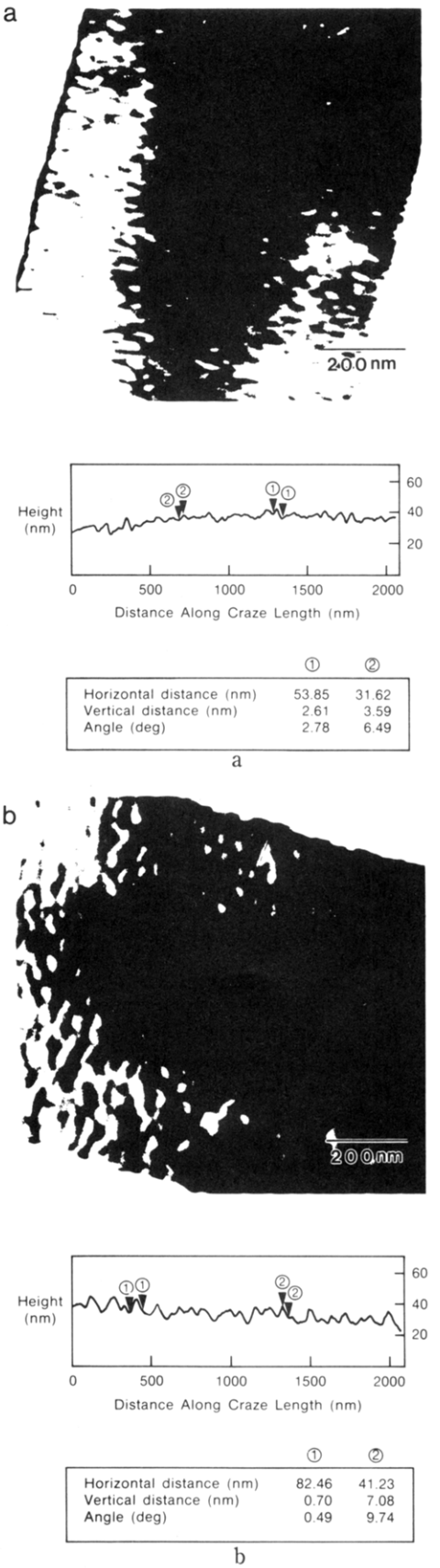

Figure 5. SFM image and height profile of a section of craze: (a) scanned approximately parallel to the fibrils; (b) scanned approximately perpendicular to the craze fibrils.

Since craze volume fraction is approximately constant with craze width,[4,6,7] a plausible mechanism for this necking process is that the length and the diameter of the fibril segments remain approximately constant but the fibril

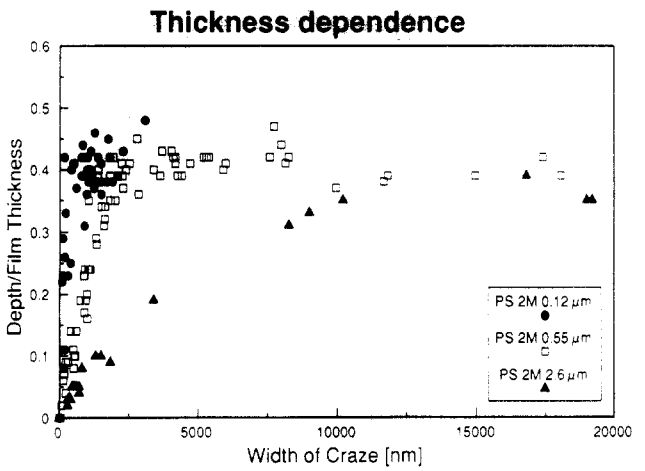

Figure 6. Maximum depth in crazes as a function of craze width for different film thicknesses.

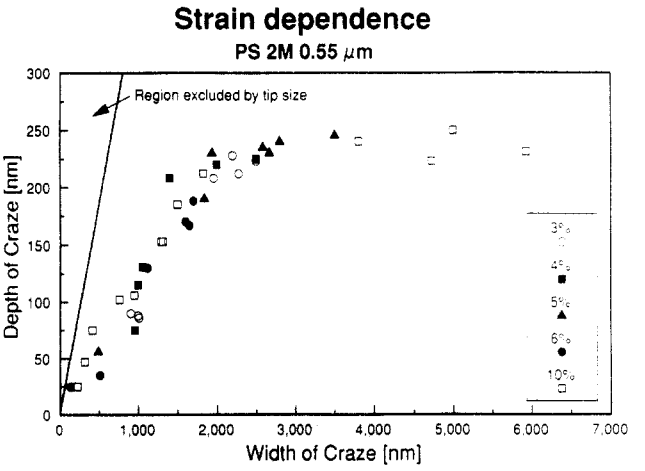

Figure 7. Effect of total applied strain on the craze depression.

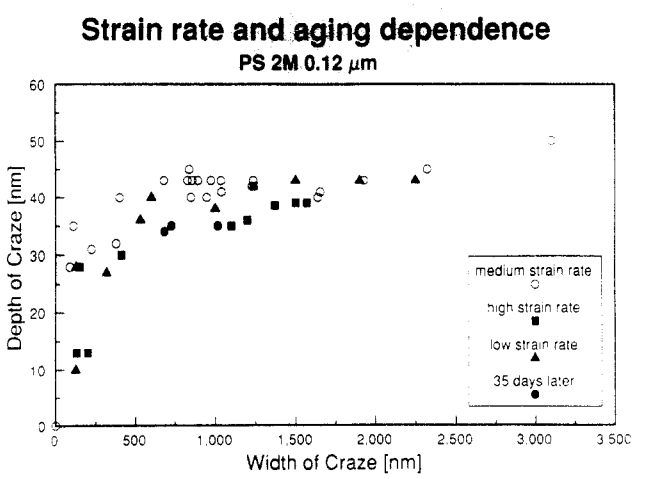

Figure 8. Effect of strain rate and aging time at ambient conditions on the craze depression. (Slow strain rate: $\dot{\epsilon} = 8.3 \times 10^{-6}$ s^{-1}. Medium strain rate: $\dot{\epsilon} = 3 \times 10^{-4}$ s^{-1}. Fast strain rate: $\dot{\epsilon} = 5 \times 10^{-2}$ s^{-1}.)

segments are aligned toward the stretch direction and the alignment causes a decrease of the fibril spacing. In this way, the craze volume fraction should be approximately constant. Figure 9 depicts the change of the fibril structure before and after this contraction. Since this proposed deformation is localized at the "hinges" where individual fibril segments join each other, it is tentatively called a "hinge deformation". When the craze width becomes larger than w_c, the fibril packing in the middle of the craze becomes so tight that no further contraction is possible there. Consequently, a neck forms and propagates toward

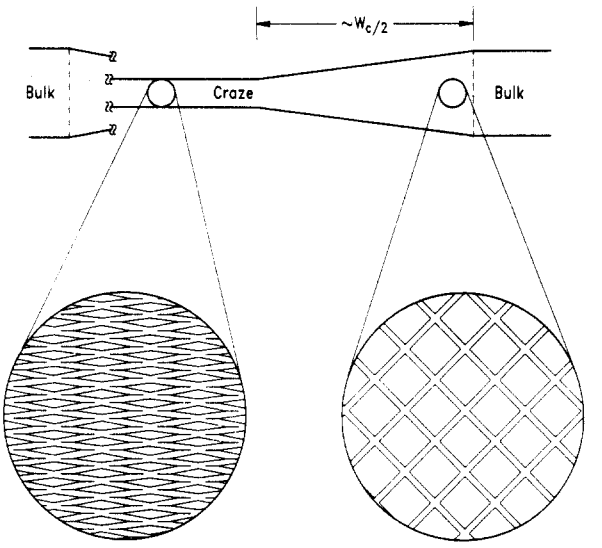

Figure 9. Schematic drawing of the cross section of the craze fibril structure in the regions near the craze boundaries and at the craze center where the fibril structure has been fully compressed.

the bulk. Due to the large observed w_c and the limited extensibility of this hinge deformation, surface drawing, however, should also take place concurrent to this fibril contraction. From the magnitude of w_c, information regarding the competition between surface drawing and fibril contraction can be obtained.

3. Micromechanics of Craze Initiation and Growth. Since crazing is a micronecking process, the mechanics of crazing can be examined by the classical necking theories. The relationship between the true stress σ and true strain ϵ at the location where a craze is to be initiated can be approximated by following the approach of the conventional Considere construction.[19], In a simplified model, consider a very narrow slab of polymer, with a length of L, thickness τ_0, and width W, which is subject to a constant-rate uniaxial elongation in the width direction. When crazing starts, the load P ($P = \sigma A$, where A is the cross-sectional area) reaches a maximum, i.e., $dP \equiv d(\sigma A) = \sigma\, dA + A\, d\sigma = 0$; therefore,

$$-dA/A = d\sigma/\sigma \tag{1}$$

During the deformation, an increase of the sample width dW should be related to the width changes in the polymer bulk and that in the incipient craze. If we denote dx to be the width reduction in the polymer bulk due to fibril drawing and dH the width increase of the fibrillated structure due to the continuous deformation, dW can be expressed as

$$dW = (\lambda\, dx + dH) - dx = (\lambda - 1)\, dx + dH \tag{2}$$

where λ is the extension ratio of the craze fibrils. Since the sample length L is constant throughout the necking, the volume change dV corresponding to dW should be

$$dV = L\tau_0(\lambda - 1)\, dx + L\tau\, dH \tag{3}$$

where τ the thickness of the fibril structure. Moreover, the force acting in the fibril structure, f_c, should be equal to the drawing force, f_d, that drew fresh fibrils from the active zones. The force f_c can be approximated as

$$f_c = E_c \tau L \frac{dH}{\lambda\, dx}$$

where E_c is the effective Young's modulus of the fibril/void structure in the stretch direction. The force f_d can be expressed in terms of the craze widening rate v and the

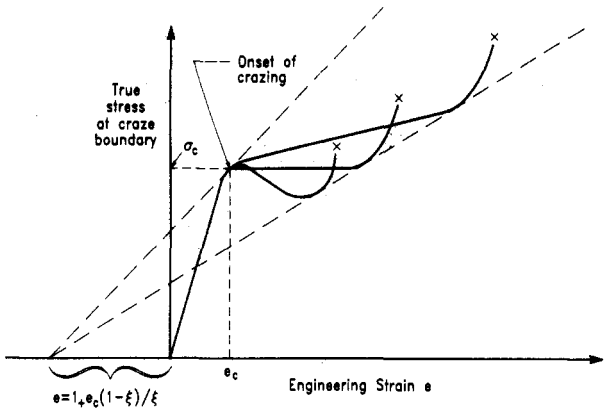

Figure 10. True stress versus engineering strain curve: a modified Considere construction.

viscosity η of the active zone according to the following:

$$f_d = \eta\beta v L \tau_0$$

where β is a geometric constant. Letting $f_c = f_d$, we have

$$dH = \frac{\eta\beta v\lambda\tau_0}{E_c\tau}\,dx \tag{4}$$

Substituting eq 4 into eqs 2 and 3, we obtained

$$dV = \tau_0 L\frac{[(\lambda-1)+\eta\beta v\lambda/E_c]}{[(\lambda-1)+\eta\beta v\lambda\tau_0/E_c\tau]}\,dW \tag{5}$$

Since $dV = W\,dA + A\,dW$, we have

$$\frac{dA}{A}+\frac{dW}{W} = \frac{(\lambda-1)+\eta\beta v\lambda/E_c}{(\lambda-1)+\eta\beta v\lambda\tau_0/E_c\tau}\frac{dW}{W} \tag{6}$$

Substituting eq 1 into eq 6 and using $d\epsilon \equiv dW/W$, we finally have

$$d\sigma/d\epsilon = \sigma\xi \tag{7}$$

where $\xi \equiv 1 - [(\lambda-1)+\eta\beta v\lambda/E_c]/[(\lambda-1)+\eta\beta v\lambda\tau_0/E_c\tau]$. This form is identical to the Considere construction except the factor ξ which is less than 1. We can use eq 7 to examine the necking point analytically in the same fashion as that using the Considere construction for the classical yielding problems. We can further replace the true strain ϵ with the engineering strain e and rewrite eq 7 as

$$\frac{d\sigma}{de} = \frac{\sigma}{(1+e)}\xi \tag{8}$$

If the width W is sufficiently small, the stress σ and strain e described above can be regarded as the local stress and local strain near the craze boundaries. The condition for craze initiation can in principle be determined from the curve of σ–e by drawing a tangent, as shown in Figure 10, from the point $e = -(1 + e(1-\xi)/\xi)$ on the strain axis to the curve. For stable neck propagation, strain hardening must take place during craze widening such that a second tangent can be drawn from the same point to the curve. The strain hardening exponent n, for the fibril contraction, can be obtained from $n = \epsilon_{crazing}\xi$ where $\epsilon_{crazing}$ can be determined from the σ–e curve. Moreover, the σ–e curves shown in Figure 10 can be viewed qualitatively as the true stress distribution along a craze. The stress distribution suggested by these curves agrees with the results by TEM stress analyses.[4,7,15]

4. Stresses inside a Craze. The stress distribution inside the crazes was obtained by using an approximation by Bridgman's necking theory.[19,20] Although the micronecking described here is a sheet-thinning process rather than a symmetric fibril drawing geometry originally assumed by Bridgman, his results nevertheless should be similar and therefore applicable to our case. Following Bridgman, the stress system inside the necked region (the craze) consists of a constant tension F in the stretching direction and a hydrostatic tension σ_h which varies with the through-thickness distance r from the central plane. The hydrostatic tension σ_h and the total tensile stress σ_z ($\equiv\sigma_h + F$) can be expressed respectively as

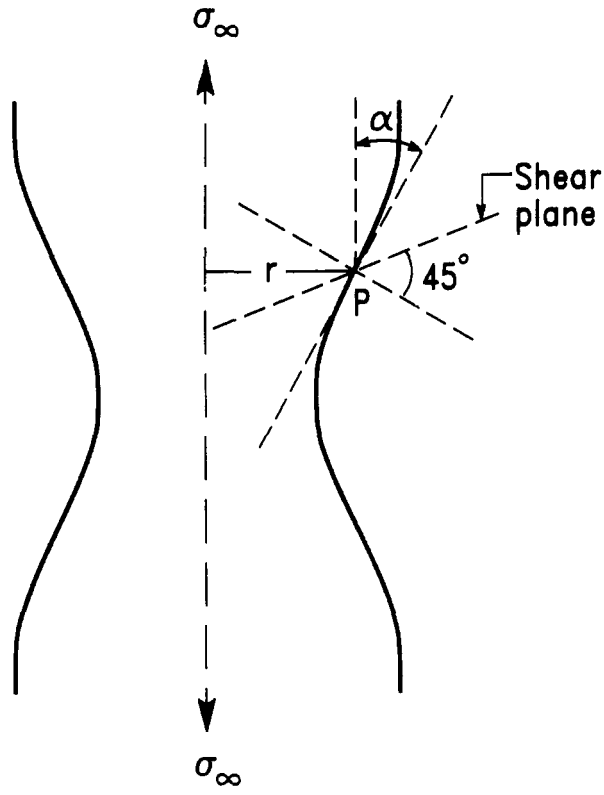

Figure 11. Schematic drawing showing the shear plane in a neck.

$$\sigma_h = F\left[\log\left(\frac{\phi^2+2\phi R-r^2}{2\phi R}\right)\right] \quad (0 \le r \le \phi) \tag{9}$$

$$\sigma_z = F\left[1+\log\left(\frac{\phi^2+2\phi R-r^2}{2\phi R}\right)\right] \quad (0 \le r \le \phi) \tag{10}$$

for a neck with a thickness ϕ and a radius of curvature R. The shear stress σ_s in the neck region can also be expressed[20] as

$$\sigma_s = \frac{\sigma_z}{2\cos^2\alpha} \tag{11}$$

where α is the surface tangent at any point P in the considered region as shown in Figure 11.

Craze breakdown can be analyzed using the information of stress distribution inside a craze. Due to the maximum σ_z at the central plane ($r = 0$), the fibrils may preferentially break down at the craze center. Once a tensile fracture starts in the center, shear can take place around the crack along the shear planes to form the so-called "cup and cone" fracture. Another possibility, however, is that the fibrils break down from the top surface at the craze/bulk boundaries where the shear stress σ_s is maximum. To demonstrate this, σ_s can be divided into two parts. The first part, σ_z, decreases slowly as the position moves toward the craze boundary because of the slow increase of r in the logarithm function. The second part, $1/(2\cos^2\alpha)$, however, increases more than compensating the decrease of σ_z due to the rapid increase of α near the boundaries.

For numerical estimations, consider a polystyrene craze with a width w larger than w_c. According to the SFM data, the surface contour α increases from zero at the craze center to more than 65° at the boundaries. In fact, the α at the boundaries is possibly higher than 65° because the measurement of α was limited by the facet angle of the SFM tip (65°). Since the reduced thickness $\phi \sim 0.3\tau_0$ and $R \sim 2.25\tau_0$, the excess of σ_h in the craze center is only approximately 7% of F. On the other hand, due to the increase of the factor $1/2 \cos^2\alpha$, σ_s increases to more than $2.8F$ at the boundaries. Evidently, due to the large stress concentration of σ_s, craze fibrils would preferentially break down at the boundaries. This is in fact exactly what was observed.[21]

The effect of film thickness on craze breakdown can be examined by using eq 11. Clearly, for a given surface tangent α, the shear stress σ_s increases with the film thickness through the dependence on ϕ. When the shear stress exceeds the fibril breakdown stress σ_b, craze breakdown and catastrophic fracture occur. Since σ_b is essentially constant with sample thickness, the maximum attainable α, hence the maximum craze width, of a mechanically stable craze decreases with the sample thickness. In a bulk specimen, the maximum craze width and maximum depression is much smaller than those permitted by a complete micronecking. This effect has to be taken into account when thin films and bulk specimens are compared for the fracture toughness that is directly related to the craze breakdown strain.

Discussion

From the dependence of craze depression on film thickness, it is clear that micronecking is the intrinsic behavior of polymer crazing, not a special surface effect. The maximum film thickness investigated here is more than 200 times the fibril diameter[8,12-14] and should be well above the regime where the surface effect is important. In the case of bulk specimens, crazes usually form as thin "plates" running perpendicular to the stretch direction. Evidence of micronecking can be found on the free surface at the interceptions with these plates, where surface depression can be detected. The development of the surface depression, however, is often terminated prematurely due to the hastened fibril breakdown and catastrophic fracture by stress increase within the crazes with sample thickness. If the craze is initiated from the interior of the bulk, the nucleation site must be associated with a triaxial tension large enough to open up the deformed materials and provide the free space for the micronecking to take place locally. In a separate experiment, it was found that when the micronecking process is prohibited, crazing in PS films is "switched off"[22] completely. We have also looked at poly(2,6-dimethyl-1,4-phenylene oxide) which is known to form shear deformation zones, rather than crazes, prior to cracking. It was found that the shear deformation zones also follow similar micronecking processes. The role of micronecking will be investigated further in the fracture of polymers and polymeric composite systems.

From the large craze depression, it is evident that fibril packing in the crazes is much denser than that previously realized. The much smaller fibril spacing may explain partly the extraordinarily fast fibril coalescence[8] when crazes are aged at the ambient conditions. The tight fibril packing also should be taken into account in the study of solvent crazing where the crack propagation is controlled by the solvent diffusion in the craze. The diffusion is strongly driven by the capillary force between the solvent and the fibrils, and smaller fibril spacing should increase the diffusion rate.

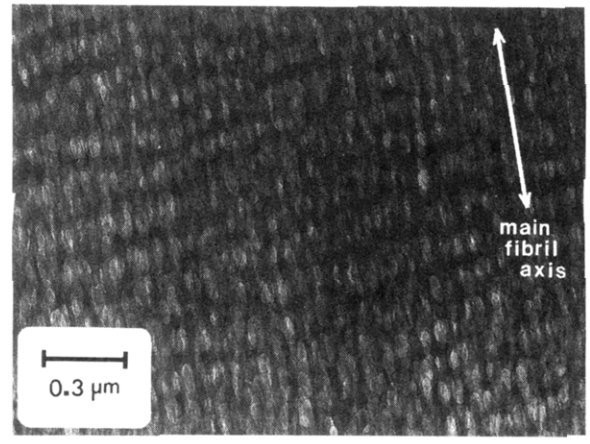

Figure 12. TEM micrograph of a wide craze showing the parallel lines along the craze length.[8]

The micronecking observation can also explain, among others, some mystery of craze microstructure. Under TEM, sometimes equispaced lines that run parallel to the craze boundaries,[8] as shown in Figure 12, were observed. These parallel lines possibly are the result of adiabatic heating generated by drawing during the micronecking process. As reported in the cases of cold-drawing of polymer filaments,[23-25] this adiabatic heating under some specific conditions can trigger a stress oscillation at the craze/bulk boundaries, establishing a periodically changing fibril drawing condition that gives rise to these almost equispaced parallel lines.

Conclusions

From the craze topography and the dependence of craze depression on the craze width, it has been shown that crazing is a micronecking process. This discovery indicates that a continuous fibril deformation takes place in concurrence with surface drawing during craze fibrillation. A hinge deformation mechanism was proposed for this continuous fibril deformation. Due to the large surface depression in the crazes, the surface-to-surface distance between craze fibrils is much smaller than that previously realized from the TEM images. This result helps to explain the fast fibril coalescence at room temperature and to examine the process of solvent crazing. The mechanics of craze initiation and breakdown can be studied using the necking theories. It is shown that the craze initiation and growth can be studied on the basis of a modified Considere construction and that the stress distribution within a craze can be investigated by using Bridgman's theory. The results from the stress analysis are in excellent agreement with the fibril breakdown behavior observed experimentally.

Acknowledgment. We acknowledge invaluable discussions with Prof. E. J. Kramer and Drs. T. W. Wu, H. R. Brown, and C. Creton.

References and Notes

(1) Rabinowitz, S.; Beardmore, P. *CRC Rev., Macromol. Sci.* **1972**, *1*, 1.
(2) Kambour, R. P. *J. Polym. Sci., Macromol. Rev.* **1973**, *7*, 1.
(3) Gent, A. N. *The Mechanics of Fracture*; Erdogon, F., Ed.; AMD, Vol. 19, ASME: New York, 1976; 55.
(4) Kramer, E. J. *Adv. Polym. Sci.* **1983**, *52/53*, 1.
(5) Kramer, E. J. *Polym. Eng. Sci.* **1984**, *24*, 761.
(6) Lauterwasser, B. D.; Kramer, E. J. *Philos. Mag.* **1979**, *A39*, 469.
(7) Wang, W.-C. V.; Kramer, E. J. *J. Mater. Sci.* **1982**, *17*, 2013.

(8) Yang, A. C.-M.; Kramer, E. J. *J. Polym. Sci., Polym. Phys.* **1985**, *23*, 1353.
(9) Miller, P.; Kramer, E. J. *J. Mater. Sci.* **1991**, *26*, 1459.
(10) Michler, G. H. *Colloid Polym. Sci.* **1985**, *263*, 462.
(11) Juska, T.; Harrison, I. R. *Polym. Eng. Sci.* **1982**, *22*, 766.
(12) Brown, H. R.; Kramer, E. J. *J. Macromol. Sci., Phys.* **1981**, *B19*, 487.
(13) Donald, A. M.; Chan, T.; Kramer, E. J. *J. Mater. Sci.* **1981**, *16*, 669.
(14) Chan, T.; Donald, A. M.; Kramer, E. J. *J. Mater. Sci.* **1981**, *16*, 676.
(15) Yang, A. C.-M.; Kramer, E. J. *J. Mater. Sci.* **1986**, *21*, 3601.
(16) Wu, S. *Polym. Eng. Sci.* **1990**, *30*, 753.
(17) Sawyer, L. C.; Grubb, D. T. In *Polymer Microscopy*; Chapman and Hall: London, 1987.
(18) Goodhew, P. J. In *Practical Methods in Electron Microscopy*; Glauert, A. M., Ed.; North-Holland-American Elsevier: Amsterdam, The Netherlands, 1972; p 137.
(19) McTegart, W. J. *Elements of Mechanical Metallurgy*; Macmillan Co.: New York and London, 1967; Chapter 1.
(20) Bridgman, P. W. *Trans. Am. Soc. Metals* **1944**, *32*, 553.
(21) Yang, A. C.-M.; Kramer, E. J.; Kuo, C. C.; Phoenix, S. L. *Macromolecules* **1986**, *19*, 2010.
(22) Yang, A. C.-M., unpublished results.
(23) Haward, R. N. *Trans. Faraday Soc.* **1943**, *39*, 267.
(24) Andrianova, G. P.; Kechekyan, A. S.; Kargin, V. A. *J. Polym. Sci., Polym. Phys. Ed.* **1971**, 1919.
(25) Richards, R. C.; Kramer, E. J. *J. Macromol. Sci., Phys.* **1972**, *B6* (1), 243.